Numerical Investigation of Radiative Heat Transfer inside a 2-D Irregular Geometry Containing Nano- and Micro-size Particles

Moghadassian, Behnam; Jafari, Mohammad ; Hafezisefat, Parinaz ; M. Hosseini, S. Mojtaba; Rezaniakolaei, Alireza

Published in:
Energy Procedia

DOI (link to publication from Publisher):
10.1016/j.egypro.2019.01.567

Publication date:
2019

Document Version
Publisher's PDF, also known as Version of record

Available online at www.sciencedirect.com

ScienceDirect

Energy Procedia 158 (2019) 5685–5691

Energy Procedia

www.elsevier.com/locate/procedia

10th International Conference on Applied Energy (ICAE2018), 22-25 August 2018, Hong Kong, China

Numerical Investigation of Radiative Heat Transfer inside a 2-D Irregular Geometry Containing Nano- and Micro-size Particles

Behnam Moghadassian[a,*], Mohammad Jafari[a], Parinaz Hafezisefat[b], Mojtaba Mirhosseini[c], Alireza Rezania[c]

[a]*Department of Aerospace Engineering, Iowa State University, Ames, Iowa, USA*
[b]*Department of Mechancial Engineering, Iowa State University, Ames, Iowa, USA*
[c]*Department of Energy Technology, Aalborg University, Pontoppidanstraede 111, 9220 Aalborg East, Denmark*

Abstract

Mie theory is very important in meteorological optics and atmospheric science. In radiative heat transfer, Mie theory is used to assess the heat transfer in participating particulate media. The effect of Mie scattering in a 2D irregular geometry is numerically investigated in this study. The medium participates in the radiative heat transfer and is filled with particulate media. FT*n* finite volume method is applied to solve the radiative transfer equation numerically. Mie theory is applied for calculation of scattering phase function in particulate media. To discretize the irregular geometries, non-orthogonal mesh is used. To calculate the radiative intensity at the cell faces, the high resolution CLAM scheme is applied. The particulate media contains particles of different sizes, ranging from 250 nanometers to 5 micrometers. Cases of scattering in media with dielectric particles and absorbing particles are considered. Also the influences of the number of particles per unit volume on the dimensionless radiative heat transfer quantities are studied.

Peer-review under responsibility of the scientific committee of ICAE2018 – The 10th International Conference on Applied Energy.

Keywords: Radiative heat transfer; Mie Theory; FT*n* finite volume method; Non-orthogonal grid; Nano particles

1. Introduction

The radiative scattering in particulate media and combustion particles find many applications in both nature and

* Corresponding author. Tel.: +1-979-492-5978;
E-mail address: behmogh@iastate.edu

Peer-review under responsibility of the scientific committee of ICAE2018 – The 10th International Conference on Applied Energy.
10.1016/j.egypro.2019.01.567

science. Scattering of sunshine in the atmosphere, red sunset and colourful rainbow, and combustion systems, are some instances of radiative heat transfer in particulate media. The most famous and general rule which governs the radiative scattering in such media is Mie theory. This theory is founded by Gustav Mie who solved the Maxwell equations to relate the scattering phase function to the medium properties. Trivic et al. [1] considered Mie scattering in the square and cubic enclosures. They successfully coupled the finite volume method (FVM) with Mie theory to perform a numerical study of the effect of anisotropic scattering on the radiative heat transfer. Khademi Moghadam et al. [2] presented the solution for transient radiative heat transfer in irregular geometries. They discretized the transient radiative transfer equation (TRTE) by FVM and compared Mie theory to isotropic approximation.

Among various methods for solving radiative transfer equation (RTE), FVM has been widely used in numerous problems such as non-orthogonal grid [3], inverse problems [4], combustion applications [5], and irregular geometries [6]. In addition to be consistent with other numerical techniques used in determining the flow and temperature fields, this method has other merits such as being easily programmable, fairly accurate and computationally cheap. However, applying FVM is accompanied with two major drawbacks due to discretizing the spatial and angular domains; i.e. false scattering and ray effect. Therefore, the attempt for improving this method to achieve higher accuracy and lower computational time has been going on since its foundation by Raithby and Chui [7]. Although these two effects are not independent from each other [8], in general, false scattering is attributed to spatial discretization and finer grids can mitigate this undesirable effect. Chai [9] and Chai et al. [10] have concluded that the FVM with Curved-Line Advection Method (CLAM) schemes gives more accurate results than FVM with step scheme in 2- and 3-D geometries. The angular discretization is responsible for the ray effect. FT*n* FVM was proposed by Kim and Huh [11]. They utilized a new angular discretization for 3-D radiative heat transfer problems. They demonstrated that the ray effect becomes less by using this angular grid in comparison with classical FVM. Together with CLAM scheme, FT*n* FVM was successfully used in radiative problem in inhomogeneous media and the irregular geometries of the combustion chambers [12, 13].

To the author's best knowledge, the study of the effects of Mie scattering in an irregular geometry has never been done. The numerical solution by coupling of Mie theory and FT*n* FVM with CLAM scheme and non-orthogonal grid is presented. Radiation heat transfer in an irregular geometry filled with particulate media is considered. Different cases of the forward, backward and isotropic scattering as well as scattering in media with real and complex index of refraction are studied.

2. Mathematical formulation for RTE solver

Modest [14] presents complete derivation of the RTE and definition of each parameter. A brief review of the RTE and the applied numerical method are given here. The radiative transfer equation in a grey emitting, absorbing and scattering media at any position, **r**, along a path, **s**, is given by:

$$\frac{dI(\mathbf{r},\mathbf{s})}{ds} = -\beta I(\mathbf{r},\mathbf{s}) + S(\mathbf{r},\mathbf{s}) \tag{1}$$

where the source function can be defined as:

$$S(\mathbf{r},\mathbf{s}) = -\kappa I_b(\mathbf{r}) + \frac{\sigma_s}{4\pi}\int I(\mathbf{r},\mathbf{s})\Phi(\mathbf{s},\mathbf{s}')d\Omega \tag{2}$$

The boundary condition for a diffusely emitting and reflecting wall can be written as follows:

$$I(\mathbf{r}_w,\mathbf{s}) = \varepsilon_w I_b(\mathbf{r}_w,\mathbf{s}) + \frac{1-\varepsilon}{\pi}\int_{\mathbf{n}_w\cdot\mathbf{s}'<0} I(\mathbf{r}_w,\mathbf{s}')\left|\mathbf{n}_w\cdot\mathbf{s}'\right|d\Omega' \tag{3}$$

The angular discretization for popular FVM and FT*n* FVM is shown in Figs. 1a and 1b, respectively. For popular

FVM the angular domain is uniformly subdivided into N_θ and N_ϕ in polar and azimuthal angles, respectively. As it can be seen, the control angles do not have the same size (they are smaller near the poles). But for FT*n* FVM the polar angle is distributed into *n* uniform subdomains where *n* is an even number. The azimuthal angle is then divided into the number of sequence of 4, 8, …, 12, 2*n*, …, 12, 8, 4 in each level of polar angle. They have almost the same size with the aspect ratio of unity. The total number of control angles is $N_s=n(n+2)$.
The discretization procedure of RTE is according to that of Chai et al. [15] and is not repeated here. By integrating the RTE (Eq. (1)) over a 2D non-orthogonal control volume (Fig. 1c) and over a control angle of FT*n* FVM (Fig. 1b), the final discretized equation can be derived as [14]:

$$a_P^l I_P^l = a_W^l I_W^l + a_E^l I_E^l + a_N^l I_N^l + a_S^l I_S^l + b^l \tag{4}$$

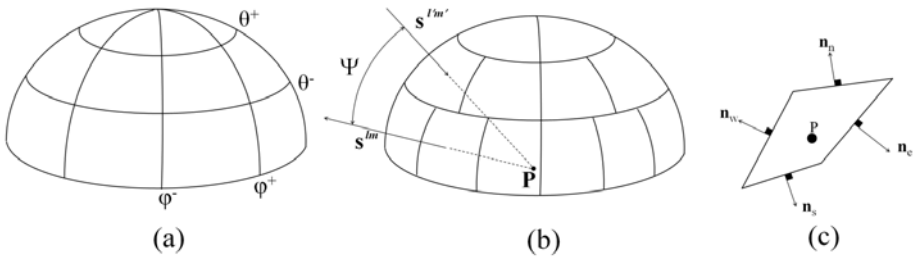

Fig 1. (a) Angular discretization for popular FVM; (b) Angular discretization for FT_6 FVM; (c) An arbitrary control volume with its representative node and surface normal vectors

The formulation of terms associated with the CLAM scheme can be found in [12, 13] and is not repeated here. The Eq. (4) is solved with an iterative approach with TDMA algorithm. The iteration stops when the following condition is satisfied:

$$\max\left|\frac{I_P^l - I_{P,old}^l}{I_{P,old}^l}\right| \le 10^{-8} \tag{5}$$

If the analytical expression for scattering phase function ($\Phi(\mathbf{s},\mathbf{s}')$) exists, the average scattering phase function in Eq. (2) can be obtained by the following relation:

$$\overline{\Phi}(\mathbf{s},\mathbf{s}') = \frac{\int_{\Delta\Omega^l}\int_{\Delta\Omega^{l'}} \Phi(\mathbf{s},\mathbf{s}')d\Omega' d\Omega}{\Delta\Omega^l} \tag{6}$$

When the integration is not feasible or $\Phi(\mathbf{s},\mathbf{s}')$ is an unknown function but its value for different $\mathbf{s}$ and $\mathbf{s}'$ can be obtained, its average can be estimated by the following formula:

$$\overline{\Phi}(\mathbf{s},\mathbf{s}') = \frac{\sum_{l_\mathbf{s}=1}^{L_\mathbf{s}}\sum_{l_{\mathbf{s}'}=1}^{L_{\mathbf{s}'}} \Phi^{l_\mathbf{s},l_{\mathbf{s}'}}\Delta\Omega^{l_\mathbf{s}}\Delta\Omega^{l_{\mathbf{s}'}}}{\Delta\Omega^l} \tag{7}$$

For particulate media of this study, the analytical expression for scattering phase function does not exist and therefore Eq. (7) must be used. Scattering phase function in any combination of $\mathbf{s}$ and $\mathbf{s}'$ is obtained by applying Mie theory. The details of complicated Mie theory are beyond the scope of this work. We have used the same

formulations and approximation method as explained in [2].

3. Results and discussion

The radiative heat transfer in the quadrilateral of Fig. 2a is studied. All walls are black. The wall number 3 is hot (E_{bw}=1 W/m^2). Other walls as well as medium are cold at 0 K. The 25×25 non-orthogonal grid is shown in Fig. 2b.

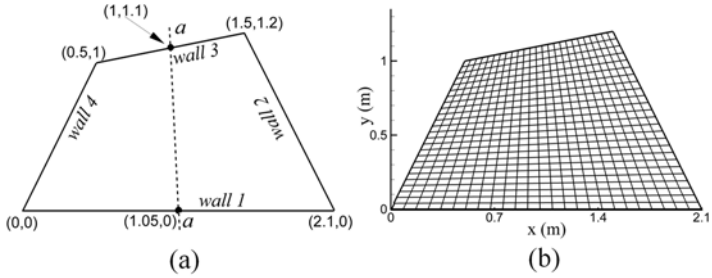

Fig 2. (a) Geometry; and (b) grid system of computational domain

First the dielectric particles of Table 1 in a purely scattering media with β=1 m^{-1} are considered. The effect of different particulate media on the dimensionless G of the line a-a, and the dimensionless heat flux on the bottom wall is studied. It is worth to mentioning that all variables in Table 1 are described in reference [1].

Table 1. Different media with real index of refraction (dielectric particles) [1]

Medium type	x_p	n	k
F1	5	1.33	0
F2	2	1.33	0
B1	1	10^8	0
B2	0.01	10^8	0

As displayed in Fig. 3a, the radiative heat flux for F1, a strong forward scattering media, is higher relative to the others. It is because more radiative energy scatters into the angles which are close to the original direction of intensity and not to its opposite direction. Therefore, a beam of ray carrying radiative intensity travelling from the hot wall to the cold ones does not lose much of its intensity due to scattering into the backward directions. The same reasoning can be applied to explain why *B2* (explained in reference [1]), a strong backward scattering media, has the lowest value of heat flux among all. In addition, the values of heat flux for the isotropic scattering media, in which the scattering is identical between all directions, lie somewhere between forward and backward scattering media as expected.

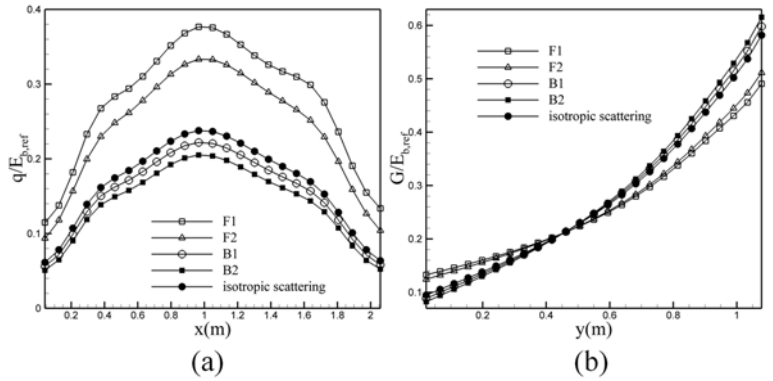

Fig 3. Results for different types media of Table 1 at x_p=2, β=1 and ω=0, (a) dimensionless heat flux on the bottom wall; and (b) dimensionless G along line a-a

Another noticeable remark in Fig. 3a is the influence of cold walls on the radiative heat flux of the bottom wall. The heat flux is low at the beginning because this region of wall 1 sees more area of the cold wall 4. When x increases, the influence of wall 4 diminishes and in the midsection of the bottom wall (around x=1m), the heat flux reaches its peak under the influence of hot wall 3. Then, due to the presence of another cold wall (wall 2) the decrement of q starts and at the end of the bottom wall, it again reaches minimum.
In Fig. 3b the dimensionless G is displayed along the centerline. As it can be seen, the difference between minimum and maximum of G tends to increase as the backward scattering increases. The forward scattering tends to unify the intensity field by distributing energy into forward directions. But in the backward scattering, the difference between cold and hot regions becomes more because the amount of energy which scatters into forward directions, and transfers between hot and cold regions is not as high as the radiative energy of forward scattering.
The absorbing particles are indicated in Table 2.

Table 2. Media with different complex indices of refraction [14]

Particle material	n	k
Carbon	2.20	1.12
Anthracite	2.05	0.540
Bituminous	1.85	0.220
Lignite	1.70	0.066
Ash	1.50	0.020

The particle density is N_T=10^5 particles/cm^3. Particle radius is a_p=1 μm resulting in x_p=2. The scattering phase function for different materials is shown in Fig 4a. The scattering phase function for different sizes of the carbon particles is also shown in Fig 4b. It is easily noticed that all particles have the forward scattering character because their scattering phase functions have higher values for acute angles of scattering. The peak of the function happens at Ψ=0. This forward characteristic becomes more significant for higher values of size parameter (x_p) as can be seen in Fig. 4b where the peak of the scattering phase function at Ψ=0 becomes more pronounced at higher values of x_p.

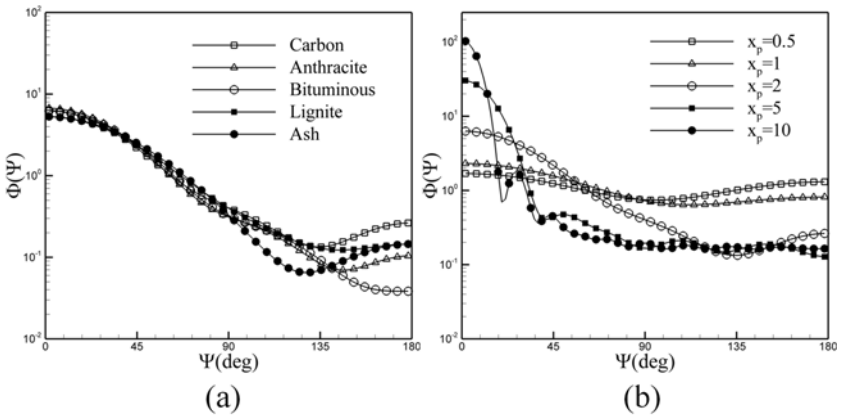

Fig 4. Scattering phase function for (a) different material of table 2 at x_p=2; and (b) for ash for different particle size parameters

Figure 5a shows the dimensionless radiative flux on the bottom surface. As shown in Fig. 4a the difference in the scattering phase function for various particles is not much. Therefore the difference in the values of radiative flux of Fig. 5a is mainly attributed to the values of β and ω. Besides the fact that the radiative intensity travels with lower changes in a media with lower extinction coefficient, the value of single scattering albedo has a significant impact on radiative transfer according to Eqs. (1) and (2). In a cold medium, the first term on the right of Eq. (2) tends to zero and the source term reduces. Therefore the ratio of σ_s to β becomes important and higher ω leads to higher radiative intensity. As a result the heat flux in a medium such as ash with lower value of β and higher value of ω must be stronger. The same condition rules the dimensionless G along the centerline of the enclosure as depicted in Fig. 5b.

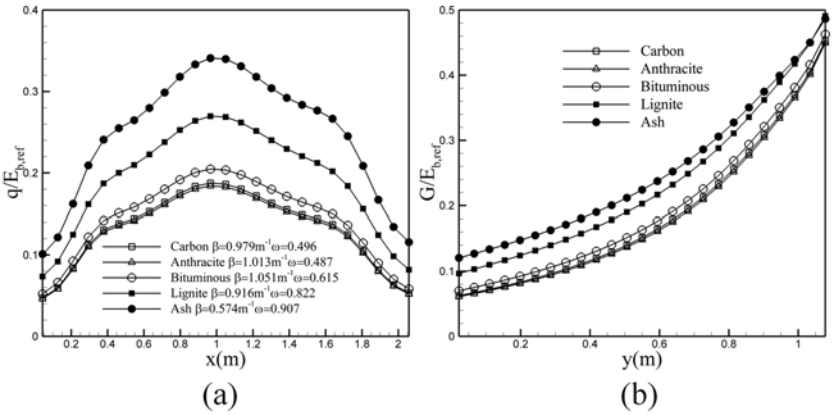

Fig 5. Results for different types media of Table 2 at x_p=2 and N_T=10^5 (particles/cm^3) (a) dimensionless heat flux on the bottom wall and (b) dimensionless G along line *a-a*

4. Conclusions

In this work the radiative heat transfer problem in particulate media is solved numerically. The computational domain is an irregular enclosure. It is assumed that the medium itself (without the particles) does not participate in radiative transfer. Particles are considered spheres whose radii vary between 250 nanometers to 5 micrometers. The effects of particle size and particle density in the media are investigated. It is found that:

- Various particulate media of table 2 have forward scattering characteristics that intensify with enhancement in particle size.
- Radiative heat flux on the cold surface is higher for forward scattering media, moreover the range of G is wider for backward scattering.
- At a constant particle diameter fly ash particles have the highest value of ω because they have the lowest absorptive index among other materials of Table 2.
- The radiative flux and integrated intensity are higher for media with smaller particles.
- For a denser media, the radiative flux is lower but the values of the directionally integrated intensity cover a wider range due to more radiative heat transfer.

References

[1] Trivic DN, O'Brien TJ, Amon CH. Modeling the radiation of anisotropically scattering media by coupling Mie theory with finite volume method. International journal of heat and mass transfer. 2004; 47(26):5765-80.
[2] Moghadam EK, Isfahani RN, Azimi A. Numerical Investigation of the Transient Radiative Heat Transfer inside a Hexagonal Furnace Filled with Particulate Medium. Am. J. Mech. Eng. 2016; 4(2):42-9.
[3] Baek SW, Kim MY, Kim JS. Nonorthogonal finite-volume solutions of radiative heat transfer in a three-dimensional enclosure. Numerical Heat Transfer, Part B. 1998; 34(4):419-37.
[4] Moghadasian M, Moghadassian B. 3 D Inverse Boundary Design Problem of Conduction-radiation Heat Transfer. Journal of Applied Sciences (Faisalabad). 2012; 12(3):233-43.
[5] Moghadassian B, Kowsary F, Mosavati M. The radiative boundary design of a hexagonal furnace filled with gray and nongray participating gases. Journal of Thermal Science and Engineering Applications. 2013; 5(3):031005.
[6] Chai JC, Lee HS, Patankar SV. Treatment of irregular geometries using a Cartesian coordinates finite-volume radiation heat transfer procedure. Numerical Heat Transfer. 1994; 26(2):225-35.
[7] Raithby GD, Chui EH. A finite-volume method for predicting a radiant heat transfer in enclosures with participating media. Journal of Heat Transfer. 1990; 112(2):415-23.
[8] Raithby GD. Evaluation of discretization errors in finite-volume radiant heat transfer predictions. Numerical Heat Transfer: Part B: Fundamentals. 1999; 36(3):241-64.
[9] Chai JC. Transient radiative transfer in irregular two-dimensional geometries. Journal of Quantitative Spectroscopy and radiative transfer. 2004; 84(3):281-94.
[10]Chai JC, Hsu PF, Lam YC. Three-dimensional transient radiative transfer modeling using the finite-volume method. Journal of Quantitative Spectroscopy and Radiative Transfer. 2004; 86(3):299-313.

[11]Kim SH, Huh KY. A new angular discretization scheme of the finite volume method for 3-D radiative heat transfer in absorbing, emitting and anisotropically scattering media. International Journal of Heat and Mass Transfer. 2000; 43(7):1233-42.
[12]Kamel G, Naceur BM, Rachid M, Rachid S. Formulation and testing of the FTn finite volume method for radiation in 3-D complex inhomogeneous participating media. Journal of Quantitative Spectroscopy and Radiative Transfer. 2006; 98(3):425-45.
[13]Borjini MN, Guedri K, Said R. Modeling of radiative heat transfer in 3D complex boiler with non-gray sooting media. Journal of Quantitative Spectroscopy and Radiative Transfer. 2007; 105(2):167-79.
[14]Modest MF. Radiative heat transfer. Academic press; 2013.
[15]Chai JC, Lee HS, Patankar SV. Finite volume method for radiation heat transfer. Journal of thermophysics and heat transfer. 1994; 8(3):419-25.